Available online at www.sciencedirect.com
SCIENCE DIRECT
Polymer 46 (2005) 8151–8156
polymer
www.elsevier.com/locate/polymer

A phenomenological model for the viscosity reductions in blends of HMMPE containing a small quantity of thermotropic liquid crystalline copolyester HBA/HQ/SA

Chi-Kwong Chan, P. Gao*

Department of Chemical Engineering, The Hong Kong University of Science and Technology, Clear Water Bay, Kowloon, Hong Kong, China

Received 19 May 2005; received in revised form 22 June 2005; accepted 22 June 2005
Available online 21 July 2005

Abstract

In this paper, we present a phenomenological model for the viscosity changes in bulk high molecular mass polyethylene (HMMPE) due to the addition of a very small quantity of a main chain longitudinal thermotropic liquid crystalline polymer (TLCP) containing flexible spacers. The chain alignment in the elongated TLCP domains causes chain alignment and disengagement in the neighboring HMMPE melt. In converging capillary flows, this occurs at a certain critical centerline velocity. After the onset of such transition, melt of elongated chain conformations forms from the center core and expands towards the capillary wall with increasing flow rates. The model successfully predicts both the drastic viscosity reduction effects and the critical yield stress in the HMMPE + TLCP blends without any adjustable parameters. Our model is also applicable to other systems that undergo flow-induced phase transitions, e.g. in biphasic liquid crystalline polymer melts.

Keywords: HMMPE + TLCP blends; Forced molecular alignment and disengagement; Converging capillary flow

1. Introduction

Blending of longitudinal thermotropic liquid crystalline polymers (TLCPs) with engineering polymers is known to lead to viscosity reductions [1–4] as well as improved mechanical [5] and barrier properties [6] of the final blend product over the pure homopolymer. In order for the TLCP to act as a property enhancer the TLCP melt should usually be in the nematic state over the same temperature range as the homopolymer is melt processable [7]. The nematic state could also be brought about by a flow-induced transition. In some cases, longitudinal TLCPs in the smectic phase have also been observed to have viscosity reduction effects in engineering polymer melts [2].

The most dramatic effect of TLCP on the bulk thermoplastics may be the viscosity changes at small TLCP loadings. Viscosity reductions of up to 70% in various engineering polymers at TLCP loadings as low as 2% have been reported by a number of authors, e.g. Kohli et al. [8]. We have observed that the use of a small quantity (as low as 0.2 wt%) of a copolyester of hydroxybenzoic acid/hydroquinone/sebacic acid terpolymer (HBA/HQ/SA) in HDPE, viscosity reductions of up to 95% may be achieved [3]. Such drastic viscosity changes have been found to be due to the intimate interactions between the two materials after the TLCP domains become highly stretched along the flow direction [4,9,10]. The mechanism of viscosity reductions in polymer blends containing TLCPs is not well understood. It is usually attributed to the deformation of TLCP droplets into elongated structures and the creation of internal 'slip surfaces'. There is, however, no theory to support this interfacial slip mechanism. A thermodynamic model based on Flory theory of LCPs developed by Blonski et al. [11] shows channeling effects where the presence of LC sequences in longitudinal LCPs causes some orientation of the non-LC polymers. A number of authors have reported that the viscosity reduction effects may also occur in the zero shear region of the blends, see for example, Kim and Denn [1], Ajji and Gignac [12]. Interfacial mixing has also been observed in LCP–polyester systems [10,12]. Our recent findings of strong interfacial interaction at the

* Corresponding author. Tel.: +852 2358 7126; fax: +852 2358 0054.
E-mail address: kepgao@ust.hk (P. Gao).

0032-3861/$ - see front matter © 2005 Elsevier Ltd. All rights reserved.
doi:10.1016/j.polymer.2005.06.095

TLCP–HMMPE interface further demonstrate that interfacial slip is absent in such systems.

The objective of this paper is to demonstrate that the bulk viscosity reductions in strongly interacting polymer blends containing longitudinal TLCPs are due to molecular disengagement in the matrix assisted by the highly aligned TLCP molecules in the dispersed phase. A phenomenological model based on the chain alignment effects in the matrix polymer due to the presence of elongated TLCP domains produced in the converging capillary flow is presented. This is analogous to the singularity effects observed in ultra-high molecular polyethylene melt first reported by Keller et al. see, for example, Kolnaar and Keller [13]. Excellent agreement between model prediction and our experimental observations will be demonstrated.

2. Experimental

2.1. Materials

The high molecular mass polyethylene, Marlex HXM TR-570 used in this study was kindly supplied by Phillips Petroleum International Inc. TR-570 has a melt flow index (MFI) of 5.5 g/10 min (ASTM D1238, 190 °C/21.6 kg). The weight average molecular weight, M_w, of TR-570 is $\sim$350, 000 kg kmol^{-1}.

The HBA/HQ/SA copolyester TLCP used here has been described before [4]. The 5 wt% dried TLCP and the high molecular mass polyethylene TR-570 was mechanically pre-mixed at ambient temperature until macroscopically homogeneous. The mixture was then extruded using a Haake Rheocord 9000 twin screw extruder at 180–190 °C. The concentration of TLCP was decreased to 1 wt% using the masterbatch method. The extrudate was palletized and kept dry inside the drying cabinet maintained at a relative humidity below 10%.

2.2. Capillary rheometry

The real time pressure versus flow rate curves on TR-570 and its blends containing 1 wt% TLCP were obtained using a piston speed controlled Göttfert Rheograph 2003A capillary rheometer with round hole capillary dies with a die entrance angle of 180°. A range of capillary die geometries was used for the study of Bagley corrections and wall slip effects. For the Bagley correction, capillary dies of diameter 1 mm and length to diameter ratios of 1, 15, 30 and 45 were used. The wall slip effects were studied using capillary dies of the same length to diameter (L/D) ratio of 30 but of diameters 0.5, 0.7, 1.3 and 1.5 mm, respectively. All data presented here have been corrected using both Bagley and Rabinowitsch corrections.

3. Model development

Capillary flows are usually considered as simple shear flows. The shear stress is the highest near the capillary die wall, where polymer chains have the highest chance to be stretched to the extended configuration [14]. This is valid only if the melt shows negligible entrance effects. The entrance effects are caused by the elongational flow due to the converging melt flow from the reservoir into the capillary die of large contraction ratios. The polymer melt along the centerline will experience the highest stretching rate. It has been observed that such effects are extremely important when anisotropic melts such as TLCPs are studied [9,10,15].

Our experimental investigations using a combination of polarized optical microscopy and TEM studies have shown that the blends of HDPE containing small concentration of TLCPs show very good interfacial compatibility. Elongated TLCP domains cause drastic chain alignment of PE chains with correlation distance more than 10 diameters of that of the TLCP domain [10]. Such strong compatibility and large viscosity differences implies that the converging flow at the die entrance is crucial for the viscosity reductions in such systems.

To account for the structural effects due to elongational flow along the centerline region, the overall melt flow characteristics are divided into three regions depending on the magnitude of the maximum fluid velocity in the capillary that is usually along the centerline in converging flows [15]. This critical fluid velocity corresponds to the maximum stretching rate of the TLCP domains at which irreversible TLCP domain elongation into slender filament takes place. The three regimes are: Region I, the fluid velocity is below the critical velocity for irreversible TLCP domain elongation, or the flow rates are low, the flow of the blends is dominated by the melt flow behavior of matrix polymer HDPE melt independent of TLCP concentration; region II, the maximum fluid velocity within the capillary reaches the critical velocity at the entrance of the capillary and irreversible elongational deformation of the TLCP domains into long slender fibrous forms begins to take place. This causes a rapid chain elongation and disengagement in the PE melt adjacent to the TLCP domains. Consequently, a region of low viscosity melt will be formed in the center core of the capillary die. This center region expands as the flow rate increases until all fluid within the capillary is filled with such melt. Region III, after all low viscosity fluid is formed across the entire capillary die diameter, homogeneous melt flow corresponding to the low viscosity melt may be assumed again. A schematic illustration of the melt structure and velocity profile evolution during flow is shown in Fig. 1(a) and (b).

For simplicity, the radial distribution of velocity profile of the extended chains is termed as ‘pattern A’ and ‘pattern B’ that of the random coil chains. In region I, the PE chains remain in the random coil configuration

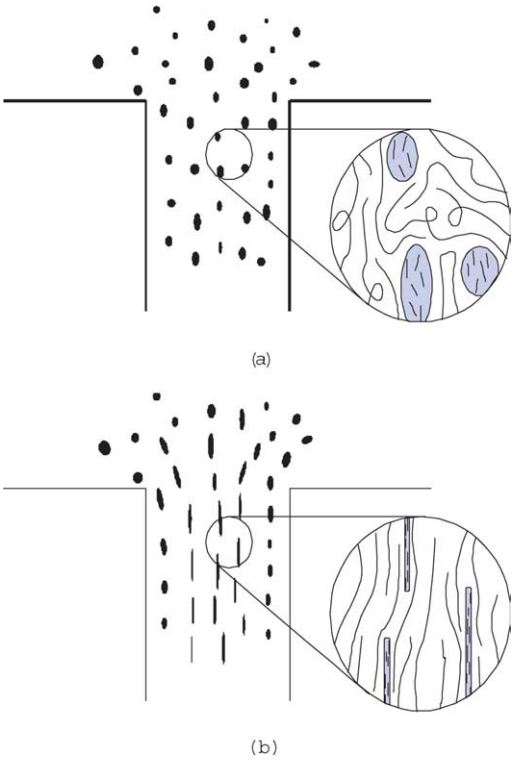

Fig. 1. Schematic diagram illustrating the chain configuration changes in the PE melt due to converging flow in the presence of highly elongated TLCP domains. (a) Isotropic structures where the dispersed TLCP droplets are nearly spherical; and (b) After the onset of chain disengagement, where the dispersed TLCP droplets are of fibrous morphology.

and produce pattern B flow profile (Fig. 2(a)). As the centerline velocity, u_0 exceeds a critical value, $u_{0,cr}$, the corresponding elongation rate, $\dot{\varepsilon}$, is high enough to stretch the PE chains along the center core from the random coil configuration to the extended chain configuration [12]. Then, pattern A starts to develop in the center core and the melt transforms into the binary flow pattern (Fig. 2(b)). As $\dot{\gamma}_{ap}$ further increases, the pattern A expands towards the die wall until it touches the capillary die wall. At this point, region III assumes which is characterized by pattern A profile (Fig. 2(c)).

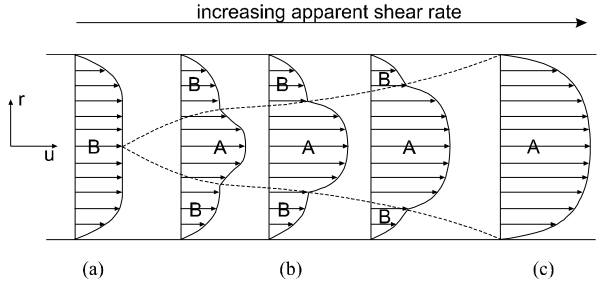

Fig. 2. Schematic diagram illustrating the flow regimes characterized by alternating flow patterns A and B as a function of maximum fluid velocity developed from the center region. (a) Region I, a homogeneous highly viscous melt where the maximum fluid velocity is below the critical velocity; (b) region II, the melt in the center region flows at velocities above the critical velocity for chain disengagement.

3.1. Velocity profiles

From the momentum equation, the shear stress, τ, at an arbitrary radius r, inside a round-hole capillary of radius R and length L is proportional to the overall pressure drop gradient, $\Delta P/L$, as shown in Eq. (1),

$$\tau = \frac{\Delta P}{L}\frac{r}{2} \tag{1}$$

Therefore, the stress at the wall and stress at radius r are related by

$$\frac{\tau_w}{\tau} = \frac{R}{r} \tag{2}$$

Substitution of the power-law constitutive relation,

$$\tau = \frac{\Delta P}{L}\frac{r}{2} = K\left(-\frac{du}{dr}\right)^n \tag{3}$$

where K and n are the power-law constants, respectively.

The velocity profile inside the capillary can be obtained by the integration of Eq. (3) to give

$$-u = \left(\frac{\Delta P}{2LK}\right)^{1/n}\frac{n}{n+1}r^{(n+1)/n} + C \tag{4}$$

where C is an arbitrary integration constant.

Using the non-slip boundary conditions at wall, i.e. $u=0$ at $r=R$, in Eq. (4), one obtains the velocity profiles in regions I (Fig. 2(a)) and III (Fig. 2(c)):

$$u_B = C_B C_{R,B}\left[1 - \left(\frac{r}{R}\right)^{(n_B+1)/n_B}\right] \tag{5}$$

where $C_B = (\Delta P/2K_B L)^{1/n_B}(n_B/(n_B+1)) = ((3n_B+1)/4(n_B+1))(\dot{\gamma}_{ap}/R^{1/n_B})$ and $C_{R,B} = R^{(n_B+1)/n_B}$

$$u_A = C_A C_{R,A}\left[1 - \left(\frac{r}{R}\right)^{(n_A+1)/n_A}\right] \tag{6}$$

where $C_A = (\Delta P/(2K_A L))^{1/n_A}(n_A/(n_A+1)) = ((3n_A+1)/4(n_A+1))(\dot{\gamma}_{ap}/R^{1/n_A})$ and $C_{R,A} = R^{(n_A+1)/n_A}$.

In Eqs. (5) and (6), we have substituted wall shear rate by the usual apparent shear rates by convention using the Rabinowitsch relation

$$\dot{\gamma}_w = \frac{1}{4}\left(3 + \frac{1}{n}\right)\dot{\gamma}_{ap} \tag{7}$$

Substitution of Eq. (7) into Eq. (3) gives the relation between the power-law parameter K' in terms of apparent shear rate, $\dot{\gamma}_{ap}$, and the power-law parameter K in terms of wall shear rate, $\dot{\gamma}_w$

Table 1
Power-law parameters of flow curves at the lower and higher viscous power-law regions

Pattern	n	K'	K
A	0.4322	11,912	10,536
B	0.404	38,408	33,833

Table 2
Observed and simulated $\tau_{w,cr}$ and the back calculated $u_{0,cr}$

Die diameter (mm)	Observed $\tau_{w,cr}$ (MPa)	Back calculated $u_{0,cr}$ (m s^{-1})	Simulated $\tau_{w,cr}$ (MPa)
0.5	0.136	0.0023	0.130
0.7	0.110	0.0019	0.113
1.5	0.080	0.0018	0.083

$$K' = K\left[\frac{1}{4}\left(3+\frac{1}{n}\right)\right]^n \tag{8}$$

All power-law parameters K, K' and n are obtained directly by fitting to the experimental data in Fig. 4 and listed in Table 1.

The velocity profile for the binary flow region II (Fig. 2(b)) is obtained by assuming interfacial continuity in velocity and shear stress and is given by:

$$u = u_I + C_A C_{R,A}\left[\left(\frac{r_I}{R}\right)^{(n_A+1)/n_A} - \left(\frac{r}{R}\right)^{(n_A+1)/n_A}\right] \quad \text{for } r < r_I \tag{9}$$

and

$$u = C_B C_{R,B}\left[1 - \left(\frac{r}{R}\right)^{(n_B+1)/n_B}\right] \quad \text{for } r_I \le r \le R \tag{10}$$

where

$$u_I = C_B C_{R,B}\left[1 - \left(\frac{r_I}{R}\right)^{(n_B+1)/n_B}\right] \tag{11}$$

The radial position r_I is computed by iteration of r_I until the

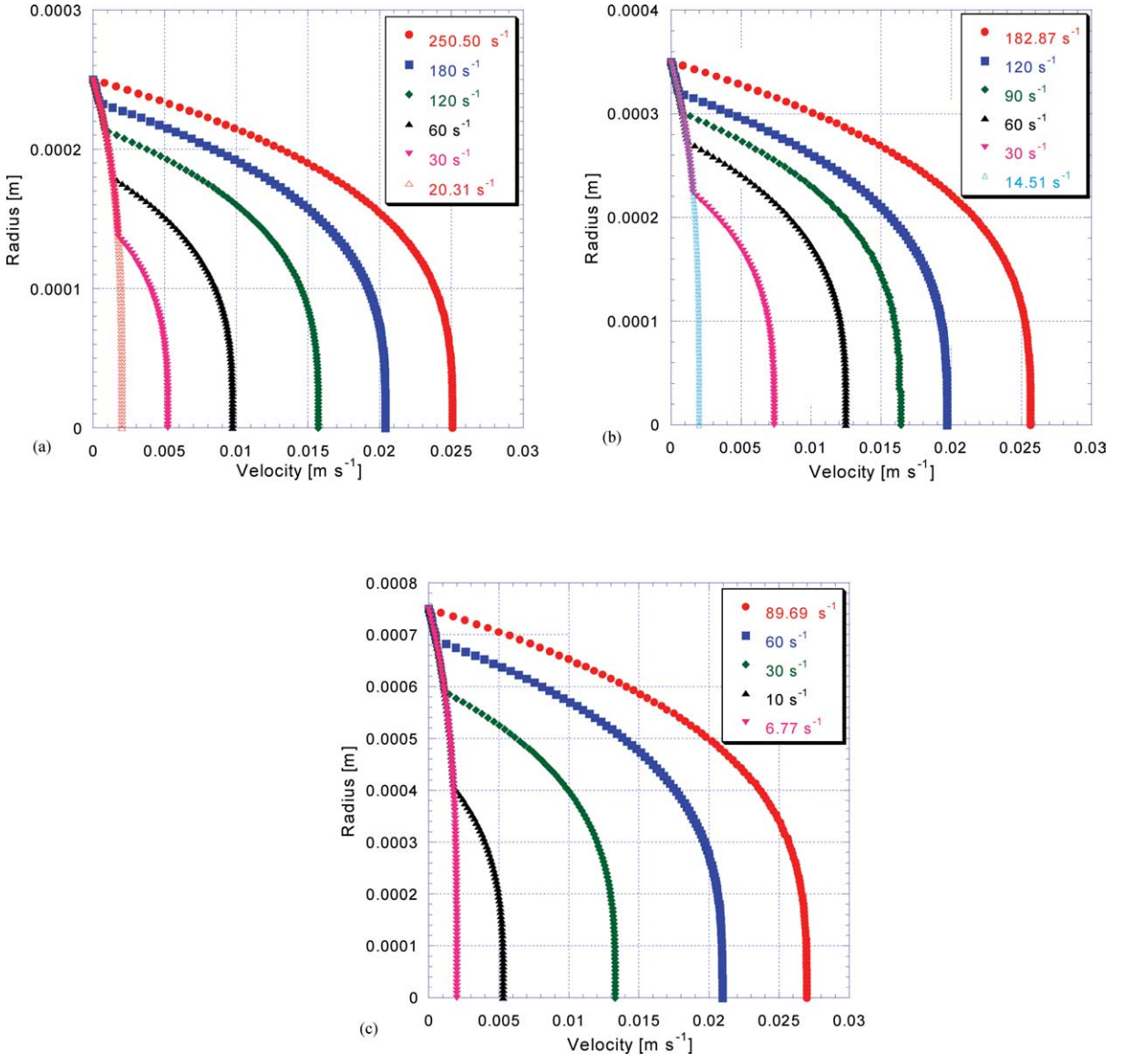

Fig. 3. Velocity profile development in region II of flow at different capillary die diameters. (a) $d=0.5$; (b) $d=0.7$ and (c) $d=1.5$ mm.

Table 3
Predicted lower and upper limits of apparent shear rates of the constant τ_w plateau region for each capillary die

Die diameter (mm)	Lower $\dot{\gamma}_{ap}$ limit (s^{-1})	Upper $\dot{\gamma}_{ap}$ limit (s^{-1})
0.5	20.31	250.50
0.7	14.51	182.87
1.5	6.77	89.70

volumetric flow rate, Q, obtained from Eq. (12) is satisfied.

$$Q = \int_0^R u 2\pi r dr \tag{12}$$

3.2. Critical centerline velocity

If the transition from random coil to the extended structure is due to chain elongation, the minimum velocity, $u_{0,cr}$, for inducing such structure changes is expected to be independent of capillary diameter. At the onset of such transition, the critical velocity can be obtained readily by substituting $r=0$ in Eq. (5):

$$u_{0,cr} = C_B C_{R,B} = \frac{3n_B + 1}{4(n_B + 1)} R\dot{\gamma}_{ap,cr} \tag{13}$$

where $\dot{\gamma}_{ap,cr}$ refers to the critical apparent shear rate at the onset of transition to region II flow. From Eq. (13), it is immediately clear that the $\dot{\gamma}_{ap,cr}$ is inversely proportional to the capillary die diameter or radius.

With the availability of $u_{0,cr}$, the critical shear stress at wall, $\tau_{w,cr}$, can then be readily calculated

$$\tau_{w,cr} = K_B \dot{\gamma}_{ap,cr}^{n_B} = K_B \left(\frac{4(n_B + 1)}{3n_B + 1} \frac{u_{0,cr}}{R} \right)^{n_B} \tag{14}$$

where the parameters are as tabulated in Table 1. From the observed $\tau_{w,cr}$ at different capillary die diameters, the $u_{0,cr}$ can be back calculated using Eqs. (13) and (14). The corresponding $\tau_{w,cr}$ and calculated $u_{0,cr}$ are tabulated in Table 2. It is found that the calculated $u_{0,cr}$ is independent of capillary die diameter with the value of ~ 0.002 m s^{-1}. Therefore, $u_{0,cr}$ is set to be 0.002 m s^{-1} and used to simulate the $\tau_{w,cr}$ and the velocity profiles for each capillary die diameter. The simulated $\tau_{w,cr}$ are also listed in Table 2 and agree very well to the observed values (Table 3).

4. Model predictions

4.1. Velocity profiles

The velocity profile developments of for fluid flowing through capillary dies of diameters 0.5, 0.7 and 1.5 mm versus apparent shear rates are shown in Fig. 3. As $\dot{\gamma}_{ap}$ increases, the center core region characterized by the low viscosity melt flow characteristics or 'pattern A' expands from the center core towards the die wall. Close to the wall, the velocity profiles are independent of apparent shear rates and are characterized by 'pattern B'. This implies that the shear rates at wall are independent of flow rates of fluid during the melt structure transition period. Consequently, the wall shear stresses will remain constant throughout this transition period. In addition, Fig. 3 also indicates that the onset of completion of the transition is also inversely proportional to the capillary die diameter.

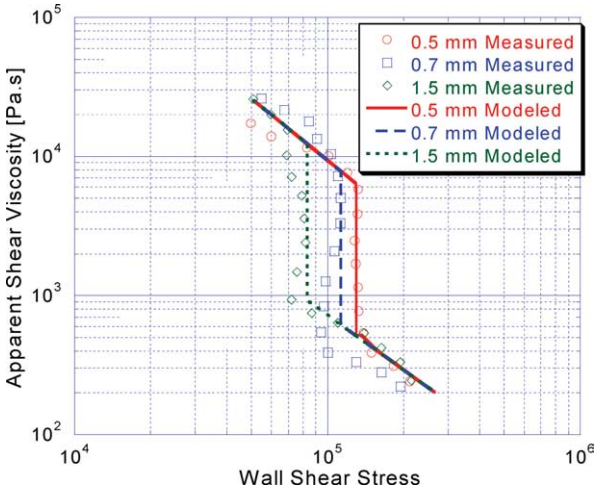

Fig. 4. Comparison of the modeled flow curves with experiments for 0.5, 0.7 and 1.5 mm die diameter but constant $L/D=30$ for the 1 wt% TLCP/HMMPE blends at 190 °C.

4.2. Flow curves simulation

The flow curves of the TLCP/HDPE blends are divided into three regimes. In regions (I) and (III), simple power-law constitutive relations are assumed. The experimental data together with the power-law constitutive model predictions are shown in Fig. 4. The flow curves in region (II) are obtained using the velocity profiles together with the power-law parameters tabulated in Table 1 and also plotted in Fig. 4.

The experimental data obtained using capillary dies of $L/D=30$ but of different capillary die diameters 0.5, 0.7 and 1.5 mm are plotted together with the model predictions in Fig. 4. An excellent agreement between model predictions and experimentally measured flow curves are obtained.

5. Conclusions

A binary flow pattern model has been proposed in this study to simulate the rheological responses of the PE+ TLCP blend. The constant τ_w plateau region has been modeled as the expansion of the melt of extended chain configurations in the center region of the capillary dies. With no adjustable parameters, the model successfully

predicts both the onset of transition and the completion of transition to the extended chain flow regime.

Elongation and orientation of the enclosed TLCP domains have been proposed to be necessary for viscosity reductions in melt containing TLCPs [2,4,12,16]. The interfacial studies carried out by us have demonstrated strong chain anisotropy in PE melt due to the presence of highly aligned TLCP molecules within the elongated TLCP domains induced by flow. The success of our model prediction for the first time gives a very simple verification such hypothesis. The model has also direct relevance to systems exhibiting shear induced phase transitions, e.g. biphasic liquid crystalline polymer melts.

Acknowledgements

The support of a grant by the Hong Kong Research Grants Council (HKUST 6121/99P) is gratefully acknowledged.

References

[1] Kim WN, Denn MM. Properties of blends of a thermotropic liquid crystalline polymer with a flexible polymer (Vectra/PET). J Rheol 1992;36:1477–98.
[2] Brostow W, Sterzynsk T, Triouleyre S. Rheological properties and morphology of binary blends of a longitudinal polymer liquid crystal with engineering polymers. Polymer 1996;37:1561–74.
[3] Whitehouse C, Gao P, Lu XH, Chai CK. The viscosity reducing effect of very low concentrations of a thermotropic copolyester in a matrix of HDPE. Polym Eng Sci 1997;37:1944–58.
[4] Chan CK, Whitehouse C, Gao P, Chai CK. Flow induced chain alignment and disengagement as the viscosity reduction mechanism within TLCP/HDPE blends. Polymer 2001;42:7847–56.
[5] Handlos AA, Baird DG. Processing and associated properties of in situ composites based on thermotropic liquid crystalline polymers and thermoplastics. J Macromol Sci, Rev Macromol Chem 1995;C35:183–238.
[6] Weinkauf DH, Paul DR. Effects of structural order on barrier properties. In: Koros WJ, editor. Barrier polymers and structures. ACS Symposium Series 423. Washington, DC: ACS; 1990 [chapter 3].
[7] Cogswell NF, Griffin BP, Rose JB. Compositions of melt-processable polymers having improved processability, US Patent 4,386,174; 1983 and 4,438,236; 1984.
[8] Kohli A, Chung N, Weiss RA. Polym Eng Sci 1989;29:573.
[9] Chan CK, Whitehouse C, Gao P. The effect of TLCP melt structure on the bulk viscosity of HMMPE. Polym Eng Sci 1999;39:1353–64.
[10] Chan CK, Gao P. Shear-induced interactions in blends of HMMPE containing a small quantity of thermotropic liquid crystalline copolyester HBA/HQ/SA. Submitted for publication.
[11] Blonski S, Brostow W, Jonah DA, Hess M. Solubility and miscibility in ternary systems: Polymer liquid crystal + flexible polymer + solvent. Macromolecules 1993;26:84–8.
[12] Ajji A, Gignac PA. Rheology and morphology of some thermotropic blends with a liquid crystalline copolyester. Polym Eng Sci 1992;32:903–8.
[13] Kolnaar JWH, Keller A. A singularity in the melt flow of polyethylene with wider implications for polymer melt flow rheology. J Non-Newtonian Fluid Mech 1997;69:71–98.
[14] Utracki LA, Walsh DJ, Weiss RA. Polymer alloys, blends and ionomers—an overview. In: Utracki LA, Weiss RA, editors. Multiphase polymers: Blends and ionomers. ACS Symposium Series 395. Washington, DC: American Chemical Society; 1989 [chapter 1].
[15] Gao P, Mackley MR, Zhao DF. The deformation and break-up of thermotropic co-polyester droplets in a molten polypropylene matrix subjecting to oscillatory shear and entry flow. J Non-Newtonian Fluid Mech 1999;80:199–216.
[16] Chang J-H, Choi B-K, Kim J-H, Lee S-M, Bang M-S. The effect of composition on thermal, mechanical and morphological properties of thermotroic liquid crystalline polyester with alkyl side-group and polycarbonate blends. Polym Eng Sci 1997;37:1564–71.